Synthesis of organic–inorganic hybrids via a high-pressure-ramp process: the effect of inorganic nanoparticle loading on structural and photochromic properties

E. Evlyukhin, L. Museur, A. Diaz-Gomez-Trevino, M. Traore, O. Brinza, Andreas Zerr, A. Kanaev

Synthesis of organic-inorganic hybrids via high-pressure-ramp process: Effect of inorganic nanoparticles loading on structural and photochromic properties

E. Evlyukhin [a], L. Museur [a], A. P. Diaz-Gomez-Trevino [b], M. Traore [b], O. Brinza [b], A. Zerr [b], A. Kanaev [b]*

a) Laboratoire de Physique des Lasers - LPL, CNRS UMR 7538, Université Paris 13, Sorbonne Paris Cité, 93430 Villetaneuse, France.

b) Laboratoire des Sciences des Procédés et des Matériaux - LSPM, CNRS, Université Paris 13, Sorbonne Paris Cité, 93430 Villetaneuse, France.

Corresponding Author

* luc.museur@univ-paris13.fr

00 33 1 49 40 37 24

ABSTRACT

Organic polymerization remains a limiting step in preparation of organic-inorganic hybrid materials with a strong concentration of the inorganic component. In this work, high-pressure-ramp process was applied to achieve pHEMA-TiO_2 nanoparticulate solids with an unprecedentedly high concentration (12 mol/l) of the inorganic component, which is four times higher than that obtained after radical polymerization induced thermally or by photons. The inorganic nanoparticles underwent morphological and structural changes with an increase of Ti concentration above 1.5 mol/l: they slightly coarsen and crystallize into anatase polymorph. The material possesses a strong photochromic response related to the electron-hole separation on the organic-inorganic interface and can store 1 e^- per 5 Ti atoms. The electron storage capacity of the titania nanoparticles decreases upon crystallization.

INTRODUCTION

Organic-inorganic hybrid materials combining useful properties of both constituent components and taking advantage of the large interface between them have been attracting a strong attention during the last decades [1, 2]. Specific functional and structural properties of the hybrids depend on their organization on the micrometric and nanometric scales as well as on the nature and extent of the organic-inorganic interface. The unlimited variety, unique structure–properties control, and compositional and shaping flexibility open a broad field of applications for hybrid materials [3]. Many routes of fabrication of the hybrid materials have been explored [4]. One of the most studied of concerns soft chemistry is the preparation and incorporation of inorganic building blocks into organic polymers. The remarkable tailoring of properties of the obtained in this way hybrids has stirred up a large interest; nowadays, these hybrids are used in optics, electronics, optoelectronics, protective coatings, sensors, etc. [2, 5-7]. In this sense, the highest concentrations of inorganic components are required in order to enhance functional response of the materials. This is notably the case in micro-optical applications where maximum concentration of inorganic components prepared of separated inorganic nanoparticles of a small size $r<<\lambda$ are required in order to design flexible, transparent refractive elements. The preparation of such hybrids is limited by their mechanical fragility [8]. In fact, while mechanical properties, mainly defined by nature and extent of the polymer network, can be reinforced by an insertion of inorganic species, an extensive increase of the inorganic component concentration weakens the solids due a steric factor of nanoparticles and leads to the polymer chains shortening. Practically, hybrids with inorganic component of <10 mol% can be achieved in this way as monolithic bulk solids, while higher inorganic contents lead to powder-like samples with an incomplete

polymerization. As a result, developments of methods for elaboration of mechanically stable organic-inorganic solids with a high concentration of preformed inorganic nanoparticles remains a challenge in hybrid materials science.

Recently, we have developed the High Pressure Ramp (HPR) method that permits ultrafast and effective radical polymerization of 2-Hydroxyethyl methacrylate (HEMA) without addition of any initiator [9]. This process is based on a formation of activated biradicals from monomers at the pressure p_1 and polymer chains growth at a pressure $p_2<p_1$ below glass transition. Because of strong material compression at high pressures, connection of the polymer chains may be promoted to overcome steric limitation imposed by dispersed inorganic nanoparticles. In this work, the HPR process is used for the preparation of bulk solid organic-inorganic hybrids and evaluated its potential for increasing the inorganic nanoparticles loading. As a model system, a pHEMA-TiO_2 hybrid containing preformed monodispersed titanium oxo-alkoxy (TOA) nanoparticles [10, 11] is examined. A strong photochromic response of pHEMA-TiO_2 hybrids [12] made possible to correlate their charge separation and storage capacity with nanoscale structural changes upon increase of the amount of nanoparticles. As a result of this correlation analysis, conclusions were drawn about suitability of the HPR method for fabrication of novel organic-inorganic hybrids with enhanced functional response.

The article is organized as follow. The elaboration process including soft chemistry inorganic synthesis of nanoparticulate HEMA-TiO_2 hybrid solutions and their HPR consolidation is described. Then, using Raman spectroscopy, the organic polymerization extent of pHEMA-TiO_2 solids is analyzed. The analysis by high resolution transmission electrons microscopy (HRTEM) allowing analyzing morphological and structural changes in

the hybrids with different inorganic concentration are described next. Finally, the photochromic properties and electrons trapping kinetics are discussed in correlation with the hybrids structure and composition.

SYNTHESIS OF HYBRIDS

The general approach to synthesis organic-inorganic hybrids with the inorganic component of dispersed titania nanoparticles has been proposed by Gorboviy et al. [10, 11]. It includes (i) elaboration of size-selected TiO_2 nanoparticles, (ii) grafting of monomers on nanoparticles surface and (iii) polymerization of the organic component. In these work we keep the preparation steps of the hybrid solutions and modified the polymerization step of the organic component by applying high pressures in the GPa range. This synthesis process is schematized in Figure 1 and its different steps are described below.

Step 1: Nanoparticles synthesis

A stable population of monodispersed titanium oxo-alkoxy (TOA) nanoparticles of radius R=2.5 nm were prepared in a sol-gel reactor with an ultra-rapid micromixing, using titanium tetra-iso-propoxyde (TTIP) precursor (Acros Organics, 98% purity) with concentration of 0.15 mol/l and distilled and filtered water in 2-propanol (Acros Organics, 99.5% purity) solution with hydrolysis ratio H=2.0 at 20.0 °C [13] (step 1 in Figure 1).

Step 2: Solvent exchange

The solvent exchange was carried out at the next step (step 2 in Figure 1). The TOA colloids in 2-propanol were mixed with HEMA (99% purity, Aldrich) in a ratio 1:A under continuous stirring and pumped overnight at 10 mbar pressure through a liquid nitrogen trap. The 2-propanol elimination was examined by an intensity decrease of the dominant

symmetric ν(CCC) Raman band situated at 818 cm^{-1} [10]. The solvent exchange does not influence the particle size and leads to the replacement of $-O^iPr$ ligands by –OEMA at the nanoparticles surface. The obtained solution of nanoparticulate precursors in HEMA is stable for 1 day in ambient atmosphere. In this state, the amount of the inorganic component in the hybrid solutions (denoted as xA) can be adjusted between 0.15 mol/l (A=1, or x1 hybrid solution) and 5.84 mol/l (A=40, or x40 hybrid solution).

Step 3: Polymerization

After the solvent exchange the hybrid solutions xA were polymerized using HPR process (step 3 in Figure 1). The process was initiated via compression to pressures $p_1 \geq 6.5$ GPa, at which $HEMA_2^{\bullet\bullet}$ biradicals were formed from HP-activated HEMA monomers. Their reactivity is however hindered by the dense glassy environment prohibiting favorable configuration adjustment of the reacting species. The polymerization occurs at pressures p_2, below that of the glass transition of ~2 GPa where the radicals become mobile. In the present experiments, HEMA-TiO_2 hybrid solutions with different TiO_2 concentrations (given by xA) were compressed in a symmetric diamond anvil cell (DAC): The DAC anvils with ~400 µm in diameter culets squeezed the sample which was confined in a hole of ~150 µm in diameter drilled in a metallic gasket pre-indented to the thickness of ~50 µm. The starting solutions were first compressed to p_1=7GPa, and then the pressure was reduced to p_2=0.5 GPa for 5 min before it was released to 1 bar. The pressures applied on samples in DAC were monitored with a precision of ±0.05 GPa using the ruby fluorescence scale.

Step 4: Sample recovery

The recovered products at atmospheric pressure were solid and transparent (step 4 in Figure 1). These hybrid samples pHEMA-TiO_2, labeled as HPXA according to the different concentrations of TiO_2 (Table 1), were used for the further analysis. It is important to notice

that the HPR process does not only provoke the radical polymerization of HEMA in absence of any initiator, but it also results in a strong contraction of solids, increasing the concentration of the inorganic component. Afterward, it was observed that the samples thickness decreased from 40 to 20 μm and the diameter 150 μm remained unchanged. As a result, the volume of the recovered samples was half that of the hybrid solutions initially loaded in DAC cell. Consequently, the inorganic component concentration in the solid hybrids was two times higher than in the hybrid solutions as specified in Table 1.

As a comparison pHEMA-TiO_2 hybrids XA were prepared via usual thermal polymerization activated by AIBN initiator, 0.1 mol% of which was dissolved in the hybrid solutions xA [10, 11]. The thermal polymerization process was conducted at 90 °C and completed over 12 hours.

RESULTS AND DISCUSSION

Polymerization efficiency

In the present experiments, Raman spectroscopy was used to monitor the conversion yield (CY) of HEMA monomers in - pHEMA-TiO_2 hybrids. Figure 2 shows Raman spectra of the liquid HEMA at atmospheric pressure, of the pure pHEMA and those of the pHEMA-TiO_2 hybrids obtained via the HPR process. The polymerization of HEMA corresponds to a progressive decrease of intensity of the C=C stretching band at 1640 cm^{-1} due to the bond opening accompanied by a consecutive increase of the C–CH_2 (1455 cm^{-1}) band intensity. The spectra were normalized to the intensity of the C=O band, which was not involved in the polymerization process. This permits a comparison of the monomer conversion yields (CY) of different hybrid samples according to the expression [14]:

$$CY = 1 - \frac{\left(I_{C=C} / I_{C=O}\right)_{\text{recovered sample}}}{\left(I_{C=C} / I_{C=O}\right)_{\text{initial HEMA}}} \quad (1)$$

where $I_{C=C}$ and $I_{C=O}$ are, respectively, areas of the ν(C=C) and ν(C=O) Raman bands. The experimental CY obtained for the HPR samples from such Raman measurements are reported in Table 1. A clear decrease of CY with an increase of the inorganic concentration was observed. In the hybrid prepared with the smallest titanium concentration, HPX2, CY attains 94 % which is not significantly different from that of the pure pHEMA obtained using the same process. However, when titanium concentration increases, CY decreases up to 10 % in the HPX40 sample with the titania concentration of 12 mol/l. A decrease of the conversion yield is commonly observed in polymers filled with clusters or nanoparticles functionalized with polymerizable ligands [15-17]. This effect is explained by crosslinking of particles, which favors a rapid growing of large macromolecules accompanied by a local increase of viscosity (the so-called “gel effect”). The entanglement of polymer chains, results in a heterogeneous composition with a relatively high content of double bonds. In our experiments, the amount of unreacted -OEMA ligands on the titania surface was expected to increase with an increase of the nanoparticles concentration, which was experimentally confirmed.

In order to emphasize specificities of the HPR induced polymerization process for the synthesis of hybrids materials, the CY of pHEMA-TiO_2 hybrids obtained via the HPR process with those obtained via the standard thermal polymerization were compared. Raman spectra of the thermally polymerized hybrids XA are shown in supplementary Figure 1 and the results are summarized in Table 2. A comparison permits the conclusion that CY, for a given concentration C_{TiO2}, is significantly higher in HPR hybrids. For example, in samples with

an equal TiO_2 concentration of 2.92 mol/l, the CY of HPX10 (63 %) is three times higher than that of the sample X20 (19 %). In other words, the use of HP allows the increase of the concentration in inorganic nanoparticles without reducing the CY of monomers in the recovered samples. This difference in CY affects the feasibility of the hybrids with the highest concentration of an inorganic component. In fact, a low conversion yield makes thermally polymerized hybrids mechanically unstable for inorganic component concentrations of 4.5 mol/l and higher; these materials exhibit a crumbling structure and can be easily destroyed by pressing between fingers. In contrast, the HPR materials remain transparent solids up to titania concentrations as high as 12 mol/l with CY=10%.

Nanoscale morphology

The nanoscale morphology of pHEMA-TiO_2 hybrids depends on the nanoparticles amount. HRTEM images in Figure 3(a), show the presence of small inorganic nanoparticles of size 2R≈3 nm in the hybrids with relatively low inorganic concentrations such as HPX2 and HPX5. Their energy filtered imaging confirmed the presence of Ti in the nanoparticles (see the supplementary Figure S2). These elementary building units of the inorganic component correspond to the titanium oxo-alkoxy species appearing in early stages of the sol-gel synthesis at low hydrolysis ratio $h^* = 1.5$ [13]. Their assignment to nuclei has been made in recent studies by Cheng et al. [18] as a result of their stability analysis in solvents. These particles remained amorphous after the HPR polymerisation stage, as confirmed from the electron diffraction pattern shown in the inset of Figure 3(a). In contrast, nanoscale morphology of the hybrids HPX10, HPX20 and HPX40 with higher inorganic concentrations changes: the elementary nanoparticles coarsened and crystallised. The electron diffraction

pattern in Figure 3(c) indicates only a partial crystallisation of nanoparticles in the HPX10 hybrid, while the inorganic crystallisation is completed in the HPX40 hybrid shown in Figure 3(d-f). The interplane distances 0.345 nm and 0.250 nm allowed to conclude about the formation of the anatase polymorph of TiO_2 with the respective crystalline planes (101) and (103).

The observed amorphous-anatase phase transition was concentration dependent: it begins in hybrid solutions charged with titania nanoparticles at C_{Ti}=3 mol/l and completes at C_{Ti}=6 mol/l. The highest titania concentration attained in HPX40 is C_{max}=12 mol/l. Taking into account that the loose random packing of spheres corresponds to $\gamma \approx 0.60$ of the ideal density of their bulk solid counterpart [19], the bulk anatase TiO_2 concentration of C_{bulk}=50 mol/l and the polymer shell thickness δ around the TiO_2 nuclei with the radius of R=1.6 nm, the maximual concentration of the inorganic nanoparticles in the hybrids is

$$C_{Ti} = C_{bulk} \cdot \gamma \cdot \left(\frac{R}{R+\delta} \right)^3 \quad (2)$$

Assuming $C_{Ti} = C_{max}$, it can be estimated that the average thickness of the polymerized material surrounding a nanoparticle:

$$\delta = R\left(\left(C_{bulk} \cdot \gamma / C_{\max} \right)^{1/3} - 1 \right) \approx 0.6 \text{ nm} \quad (3)$$

This interparticle distance corresponds to the length of oligomers $HEMA_k$ with $k \approx 3$. The appearance of short polymer chains connecting the nanoparticles, seen in Figure 3(f), indicates that the material solidifies; however, a considerable amount of monomers remains in voids between the nanoparticles decreasing the conversion yield.

The observed concentration influence on the amorphous-anatase phase transition in TiO_2 nanoparticles can be related to the particle size effect. The size effect on crystalline phase transformations in metal oxides has been discussed in Ref. [20] and experimentally

confirmed for the anatase-rutile transformation in TiO_2 nanoparticles [21, 22]. It has been shown in the literature that a significant contribution of the surface energy inverts the phase stability and prohibits appearance of the rutile phase when particles are smaller than 14 nm. The anatase crystallisation that takes place in single amorphous TiO_2 particles of 5 nm in size, however, it requires a significant thermal activation. A considerable increase of the transformation onset temperature from 350°C to 550 °C in the aggregated nanopowders, has been reported [23]. The critical particle size allowing the anatase crystallization may be smaller than 5 nm.

The present results suggest that the transition onset pressure is related to size of the TiO_2 particles with the critical value between 3 and 5 nm. In fact, pressure plays a similar role as temperature in the activation process. Results (Figure 3) indicate that TiO_2 particles of 3 nm remain amorphous after the high pressure processing, while those of 5 nm underwent a phase transition and crystallize to the anatase polymorph. As reported previously, the hybrid solution contains 5 nm particles after the solvent exchange stage [10]. Apparently, the appearance of 3 nm particles in solid hybrids was due to disaggregation of 5 nm particles on the polymerization stage, which may have resulted from mechanical constraints induced by the polymerization process. creating a sufficient mechanical constraint. In support of this hypothesis, environmental conditions affect these larger nanoparticles, in contrast to small nuclei which remain stable [18]. The phase transition takes place at the inorganic concentration $C_{Ti} \geq 3$ mol/l. An increased titania concentration sets nanoparticles closer to each other favoring mutual contact and aggregation. As a result, the nanoparticles coarsen and crystallize reaching the size of 5 nm. With lower activation energy, this process is expected to begin at the particle contact interface and to propagate through the contact

area. The crystallization of two connected nanoparticles along (101) and (103) planes is shown in Figure 3(f).

Photochromic properties

Functional properties of the prepared hybrids are defined by the inorganic component and can be enhanced by an increase of its concentration. In particular, the inorganic component is responsible for the photochromic response, which is connected to photoinduced modifications of the material refraction and opens a way to the light control of the local refractive index [24]. Below, the photochromic response of HP hybrids is evaluated and conclusions are drawn about their suitability for applications in micro-optics.

We have performed pump-probe absorption measurements, in which the recovered samples were irradiated with a UV (pump) laser pulses at 355 nm while the photoinduced absorption was probed at the wavelength of 640 nm corresponding to the maximum of the Ti^{3+} centers absorption. The photodarkening kinetics of the HPR hybrids is shown in Figure 4. As it has been reported in previous studies [12], irradiation of pHEMA-TiO_2 hybrids in the UVA spectral range with photon energies hν>3.2 eV provokes an effective separation and trapping of photoinduced charges at the organic-inorganic interface which can be described by the following equations (4) and (5):

$$TiO_2 + h\nu \rightarrow TiO_2\,(e_{CB} + h_{VB}) \tag{4}$$

$$\left.\begin{aligned} Ti^{4+} + e_{CB} &\rightarrow Ti^{3+} \\ h_{VB} + pHEMA &\rightarrow pHEMA(h_{tr}) \end{aligned}\right\} \tag{5}$$

The hole h_{VB} escapes into the organic component while the electron e_{CB} is localized as a small polaron Ti^{3+} in the inorganic component. Because of the spatial separation, the

spontaneous recombination of charges after the trapping is negligible on a timescale of weeks. The relaxation process can be initiated by the atmospheric oxygen and the trapped electrons remained stable as long as the sample is kept under inert atmosphere. The accumulation of the trapped electrons produces a photochromic effect [12, 25]. In order to calculate the trapped electron concentrations (the right axis in Figure 4) we used the known absorption cross section of Ti^{3+} centers reported to be $\sigma_{640} = 1.3\,10^{-18}\,cm^2$ [26].

The photodarkening kinetics can be considered as an additive effect of accumulation of electrons in a single TiO_2 nanoparticle unless the interaction between the nanoparticles affects the process. Therefore, at least for low nanoparticle concentrations, the single particle contribution is assumed to dominate. As seen in Figure 4, shapes of the darkening kinetics curves of HPX2, HPX5, and HPX10 hybrids are similar. The concentration of trapped electrons is directly proportional to the titania concentration, which proves the additive character of photodarkening relating to the single particle response. In contrast, the additive response fails to describe the dose dependence of the trapped electron concentration in hybrids HPX20 and HPX40, which conveys a significant modification of the nanoscale morphology of the inorganic component in these samples. The reason could be an interaction between the particles at elevated concentrations and/or amorphous-anatase phase transition discussed above. The deviation from the additive response appears in hybrids with the inorganic nanoparticles concentrations of 6 and 12 mol/l and at UV-light doses above 0.2 kJ/cm². This indicates that a small charging by electrons proceeds similarly in all HP hybrids, whatever their inorganic components are, the 3-nm amorphous or 5-nm crystalline anatase TiO_2 particles. Consequently, charging of a thin organic interface between inorganic nanoparticles prevents the valence band (VB) holes exit and enhances the electron-hole recombination rate. According to our estimations, one 5-nm particle

accumulates about 250 electrons after 0.2 kJ/cm² irradiation, which becomes limiting for the charging of the HP40 hybrid with almost closed packing of nanoparticles. Another explanation that cannot be rejected at this stage of research is a limiting electron trapping capacity of anatase compared to amorphous TiO_2. Further studies will clarify this issue.

A physical model earlier proposed by Kuznetsov et al. [12] has been used to successfully describe the photodarkening kinetics of pHEMA-TiO_2 hybrids at relatively small irradiation doses below 0.5 kJ/cm². At the same time, it failed to explain the kinetics of HPR hybrids at higher doses up to 6 kJ/cm². The principal discrepancy concerns the process saturation explained by the so-called inner photoeffect. This effect intrinsically implies a saturation of the Ti^{3+} formation kinetics when amounts of created trapped electrons and those released from the traps and recombining with trapped holes, after absorption of UV photons, becomes equal. Such aaturation of absorbance was not observed in the present experiments. An alternative explanation was evoked earlier by Bityurin at al. [27] interpreting the kinetics of trapping as resulting from a specific interaction of the trapped electrons (Ti^{3+}) with the free electrons, which are attempting to be trapped into an empty site (Ti^{4+}). Actually, the Ti^{3+} centers distort the potential energy surface creating barriers that a CB electron has to overcome to reach the trap site. Below this point of view is considered to propose a model explaining the formation kinetics of Ti^{3+} centers under UV irradiation. It was assumed that the number of such barriers is proportional to the local trapped electrons concentration. Accordingly, the quantum yield of trapping is expressed:

$$\eta = \eta_0 \left(1 - \frac{[Ti^{3+}]}{N_{tr}}\right) \exp\left(-\frac{E}{kT}\right) \quad (6)$$

where $[Ti^{3+}]$ is number density of trapped electrons, η_0 is quantum yield of electron trapping at t=0 (when no electrons are yet trapped). The barrier height $E = E_1 \left[Ti^{3+}\right] / N_{tr}$ is

proportional to the occupancy of the trap sites with number density N_{tr} and equivalent barrier height of a single charged site E_1.

We included the above formalism of Eq.(6) in the general schema of the photoinduced charge separation processes in the pHEMA-TiO_2 hybrids presented in Figure 5. The absorption of a UV photon (1) leads to the excitation of one electron from the valence band formed of the O^{2-}(2p) orbitals to the conduction band of the Ti^{4+}(3d) orbitals in TiO_2. The CB electron can either recombines directly with the VB hole (2) or undergo trapping forming Ti^{3+} centers (3). The VB hole escaping recombination with the CB electron exits to the organic component of the hybrid (4). According to earlier experimental observations, the spontaneous relaxation of trapped electrons (5) can be disregarded on a short process timescale [12]. In the framework of this model, the experimental darkening kinetics shown in Figure 4 can be described with equations

$$\begin{aligned} \partial\left[Ti^{3+}\right]/\partial t &= \eta\left(\left[Ti^{4+}\right]_0 - \left[Ti^{3+}\right]\right)\sigma_a I \\ \partial I/\partial x &= -\left(\sigma_a\left[Ti^{4+}\right] + \sigma_b\left[Ti^{3+}\right]\right)I \end{aligned} \qquad (7)$$

With laser intensity I expressed in photons/(cm^2·s) and absorption cross-sections of $\sigma_a = 4.3\,10^{-20}\,cm^2$ and $\sigma_b = 0.52\,10^{-18}\,cm^2$ at λ=355 nm [12]. The model equations (6)-(7) with η_0=0.07, $N_{tr}/C_{T\,i} = 0.24$ and $E_1 = 130$ meV successfully described photoinduced kinetics of the HPX2, HPX5 and HPX10 hybrids and are presented by dashed lines in Figure 4. A physical significance of the proposed model is supported by the elementary barrier height of 130 meV corresponding to the Urbach's energy of titania [28]. The model rationalizes an excellent trapping capacity of the nanoparticulate HPR pHEMA-TiO_2 hybrids with the inorganic component concentration of 3 mol/l and an absolute record number density of the

trapped electrons of 10^{21} cm^{-3} attained in the HPR hybrids with unprecedentedly high inorganic component concentration of 12 mol/l.

The high electron storage capacity shows the application attractiveness of the hybrid materials realized via the HPR process. In particular, the value of 10^{21} cm^{-3} is ten times higher than that previously obtained for the thermally polymerized hybrids [12]. For comparison, in bundles of single wall carbon nanotubes [29] often referred to as a supercapacitor, an absolute electron concentration 10^{21} cm^{-3} has been estimated , which is similar to that measured in the present work. Further, we can estimate the local modification of the refraction index applying the refraction per charged centre of $a_0 = \Delta n / [Ti^{3+}] \approx$-2.4 10^{-23} cm^3 previously measured in nanoparticulate pHEMA-TiO_2 hybrids prepared via sol-gel/thermal polymerisation process [24]. Because of an important increase of the inorganic component concentration and its electron loading capacity, the electron concentration in HPX40 material can easily attain 10^{21} cm^{-3} that provokes local modification of the refraction index by $\Delta n = -0.024$, making these type of materials to valuable candidates for applications in micro-optics and optoelectronics.

Complementary to the photoinduced refraction, the linear refractive index of the prepared material can also be estimated. Titania nanoparticles with the size above 3 nm possess electronic structure of the bulk solid [30, 31]. Therefore their refraction is expected to be as high as that of the TiO_2 anatase crystals measured to be $n \approx 3$ in the visible spectral range [32]. Using the Wiener equation indicated for spherical bodies and volume additivity, the maximum refraction attained in HPX40 hybrid is estimated by

$$\frac{n_{12}^2 - n_1^2}{n_{12}^2 + 2n_1^2} = \phi_2 \frac{n_2^2 - n_1^2}{n_2^2 + 2n_1^2} \qquad (8)$$

Where n_i and ϕ_i (i=1, 2, 12) are refractive indexes and volume fractions of respectively individual components and their mixture. Taking refractive indexes of HEMA $n_1 = 1.45$ and $\phi_2 = 0.24$, we obtain $n_1 = 1.73$, which is significantly higher compared with those previously obtained in sol-gel based titania hybrids [33].

CONCLUSION

Nanoparticulate transparent photochromic pHEMA-TiO_2 hybrid materials were synthesized via sequential sol-gel and HPR processes. This method has permitted the highest inorganic component concentration of 12 mol/l, which is four times higher than that obtained after the radical-assisted polymerization induced thermally or by photons. The inorganic component of hybrid consisted of nanoparticles, which were amorphous and had a size of 3 nm at relatively low concentrations, and crystallized to the anatase polymorph and coarsen to 5 nm when the TiO_2 concentration was increased above 1.5 mol/l. The obtained material possessed a strong photochromic response related to the electron-hole separation on the organic-inorganic interface and can stored 1 e^- per 5 Ti atoms. As a result, the concentration of trapped electrons of 10^{21} cm^{-3} was measured, which corresponds to ~300 electrons per nanoparticle. The electron storage capacity of the inorganic component decreased upon crystallization. An important increase of the inorganic component concentration and its electron storage capacity suggested the refraction index increased to $n = 1.73$ and strong local light-induced modification of the refraction index $\Delta n = -0.024$ making HPR hybrids valuable candidates for fabrication of flexible micro-optical elements and applications in optoelectronics.

CHARACTERIZATION METHODS.

Raman measurements.

The polymerization of pHEMA-TiO2 hybrid materials was studied by means of Raman spectroscopy. All Raman spectra of our hybrid samples were measured at room temperature in backscattering configuration using a HR800 spectrometer equipped with a Peltier-cooled CCD detector (Horiba JobinYvon) with spectral and spatial resolutions of 0.25 cm^{-1} and 5 μm, respectively. Raman measurements were carried out for recovered samples as well as in-situ for samples compressed in the DAC. For this reason the anvils of the DAC are made of type IA diamonds preselected for their low fluorescence in the frequency region of the Raman measurements.

Transmission electron microscopy

The nanomorphology of our samples was characterised by JEOL2011 high resolution transmission electron microscope (HRTEM) operated at 200 keV with an emission type LaB_6 cathode (field emission). Moreover, a Gatan Imaging Filter 2000 system built into the TEM allowed access to element maps by energy filtered transmission electron microscopy (EFTEM). The resolution of the energy filter is 1 eV and the lateral resolution is 1 nm.

Pump-probe optical absorption experiment.

The pHEMA-TiO_2 hybrids are photosensitive materials subject to photodarkenning under UV irradiation. We have analysed this effect by means of a pump-probe experiment in which the absorbance of the sample at 640 nm is monitored as function of the UV (355 nm) irradiation doze. The experimental setup is shown in supplementary Figure 2.A high repetition rate diode pump solid state (DPSS) UV laser delivers pulses of 7 ns at 355 nm with

a mean power of 10 mW. The UV beam is collimated by a first lens (L1) with a 20 cm focal distance and focused on the sample thought a second long focal lens (L2) with a 75 cm focal distance. This combination of lenses ensures a Gaussian shape of the UV beam on the sample inside DAC with a radius of ~30 µm. A variable attenuator (LBA) designed for linearly polarized laser beam is placed between lenses L1 and L2 in order to adjust the UV laser power on the sample. The UV power on the sample is carefully monitored by a power meter calibrated on purpose. The probe beam at 640 nm is delivered by a CW fibred-diode laser (from Thor labs) and focus on a spot with a radius of ~8µm on the sample inside the DAC by a short focal lens (L3). The beam transmitted through the sample is collimated (L4) and monitored by a Si photodiode (D1). The superposition of UV and 640 nm laser beams is carefully controlledwith a camera before each experiment.

ACKNOLEDGMENTS

ANR (Agence Nationale de la Recherche) and CGI (Commissariat à l'Investissement d'Avenir) are gratefully acknowledged for their financial support of this work through the Labex SEAM (Science and Engineering for Advanced Materials and devices) ANR 11 LABX 086, ANR 11 IDEX 05 02. The Federative Structure IFR “Paris Nord Plaine de France” on materials science is gratefully acknowledged.

ADDITIONAL INFORMATION

Competing Financial Interest: The authors declare no competing financial interests.

REFERENCES

1. G. Kickelbick, ed., *Hybrid Materials : Synthesis, characterization and apllications*, Wiley-VCH Verlag GmbH & Co, Weinheim, 2006.
2. C. Sanchez, P. Belleville, M. Popall and L. Nicole, *Chem. Soc. Rev.*, 2011, **40**, 696-753.
3. C. Sanchez, B. Julian, P. Belleville and M. Popall, *Journal of Materials Chemistry*, 2005, **15**, 3559-3592.
4. P. Gómez-Romero and C. Sanchez, Wiley-VCH Verlag GmbH & Co. KGaA, 2003.
5. C. Sanchez, B. Lebeau, F. Chaput and J. P. Boilot, *Adv. Mater.*, 2003, **15**, 1969-1994.
6. P. Escribano, B. Julian-Lopez, J. Planelles-Arago, E. Cordoncillo, B. Viana and C. Sanchez, *Journal of Materials Chemistry*, 2008, **18**, 23-40.
7. C. Sanchez and B. Lebeau, *MRS Bulletin*, 2001, **26**, 377-387.
8. F. Mammeri, E. L. Bourhis, L. Rozes and C. Sanchez, *J. Mater. Chem.*, 2005, **15**, 3787-3811.
9. E. Evlyukhin, L. Museur, M. Traore, C. Perruchot, A. Zerr and A. Kanaev, *Scientific Reports*, 2016, **5**, 18244.
10. P. Gorbovyi, A. Uklein, S. Tieng, O. Brinza, M. Traore, K. Chhor, L. Museur and A. Kanaev, *Nanoscale*, 2011, **3**, 1807-1812.
11. P. Gorbovyi, A. Uklein, M. Traore, L. Museur and A. Kanaev, *Mater. Res. Express*, 2014, **1**.
12. A. I. Kuznetsov, O. Kameneva, N. Bityurin, L. Rozes, C. Sanchez and A. Kanaev, *PCCP*, 2009, **11**, 1248-1257.
13. R. Azouani, A. Soloviev, M. Benmami, K. Chhor, J. F. Bocquet and A. Kanaev, *The Journal of Physical Chemistry C*, 2007, **111**, 16243-16248.
14. E. Evlyukhin, L. Museur, M. Traore, S. M. Nikitin, A. Zerr and A. Kanaev, *The Journal of Physical Chemistry B*, 2015, **119**, 3577-3582.
15. J. Kreutzer, X.-H. Qin, C. Gorsche, H. Peterlik, R. Liska and U. Schubert, *Materials Today Communications*, 2015, **5**, 10-17.

16. Y. Gao, F. R. Kogler and U. Schubert, *J. Polym. Sci., Part A: Polym. Chem.*, 2005, **43**, 6586-6591.

17. U. Schubert, *Chem. Soc. Rev.*, 2011, **40**, 575-582.

18. K. Cheng, K. Chhor and A. Kanaev, *Chem. Phys. Lett.*, 2017, **672**, 119-123.

19. F. A. Dullien, *Porous media: fluid transport and pore structure*, Academic press, 2012.

20. A. Navrotsky, *Geochem. Trans.*, 2003, **4**, 34-37.

21. J. Banfield, *J. Mater. Chem.*, 1998, **8**, 2073-2076.

22. M. Bouslama, M. Amamra, Z. Jia, M. Ben Amar, K. Chhor, O. Brinza, M. Abderrabba, J.-L. Vignes and A. Kanaev, *Acs Catalysis*, 2012, **2**, 1884-1892.

23. O. Khatim, M. Amamra, K. Chhor, A. Bell, D. Novikov, D. Vrel and A. Kanaev, *Chem. Phys. Lett.*, 2013, **558**, 53-56.

24. A. Uklein, P. Gorbovyi, M. Traore, L. Museur and A. Kanaev, *Opt. Mater. Express*, 2013, **3**, 533-545.

25. L. Museur, P. Gorbovyi, M. Traore, A. Kanaev, L. Rozes and C. Sanchez, *J. Lumin.*, 2012, **132**, 1192-1199.

26. A. Kuznetsov, O. Kameneva, L. Rozes, C. Sanchez, N. Bityurin and A. Kanaev, *Chem. Phys. Lett.*, 2006, **429**, 523-527.

27. N. Bityurin, A. I. Kuznetsov and A. Kanaev, *Appl. Surf. Sci.*, 2005, **248**, 86-90.

28. V. Nadtochenko, N. Denisov, A. Gorenberg, Y. Kozlov, P. Chubukov, J. Rengifo, C. Pulgarin and J. Kiwi, *Applied Catalysis B: Environmental*, 2009, **91**, 460-469.

29. D. N. Futaba, K. Hata, T. Yamada, T. Hiraoka, Y. Hayamizu, Y. Kakudate, O. Tanaike, H. Hatori, M. Yumura and S. Iijima, *Nat. Mater.*, 2006, **5**, 987.

30. S. Monticone, R. Tufeu, A. Kanaev, E. Scolan and C. Sanchez, *Appl. Surf. Sci.*, 2000, **162**, 565-570.

31. N. Satoh, T. Nakashima, K. Kamikura and K. Yamamoto, *Nature nanotechnology*, 2008, **3**, 106.

32. H. Tang, H. Berger, P. Schmid and F. Levy, *Solid State Commun.*, 1994, **92**, 267-271.

33. B.-y. Wu and D.-h. Zhang, *Chin J polymer Science*, 2004, **22**, 247-251.

Samplename	Volume of nanoparticles suspension mixed with 5 ml of HEMA (ml)	TiO_2 concentration in hybrid solutions (Mol/l)	TiO_2 concentration in solid hybrids after HPR (Mol/l)	Conversion yield of HEMA monomers (%)
HP-X2	10	0.29	0.58	94
HP-X5	25	0.73	1.46	78
HP-X10	50	1.46	2.92	63
HP-X20	100	2.92	5.84	37
HP-X40	200	5.84	11.68	10

Table 1: Titania concentration and conversion yield of HEMA monomers in pHEMA-TiO_2 hybrid materials synthesized by the HPR induced polymerization (see text for details)

Samplename	Volume of nanoparticles suspension mixed with 5 ml of HEMA (ml)	TiO_2 concentration in hybrid solutions (mol/l)	Conversion yield of HEMA monomers (%)
X10	50	1.46	50
X20	100	2.92	19
X40	200	5.84	Not mechanically stable

Table 2: Titania concentration and conversion yield of HEMA monomers in pHEMA-TiO_2 hybrid materials synthetized at ambient pressure from a thermally activated radical initiator (see text for details)

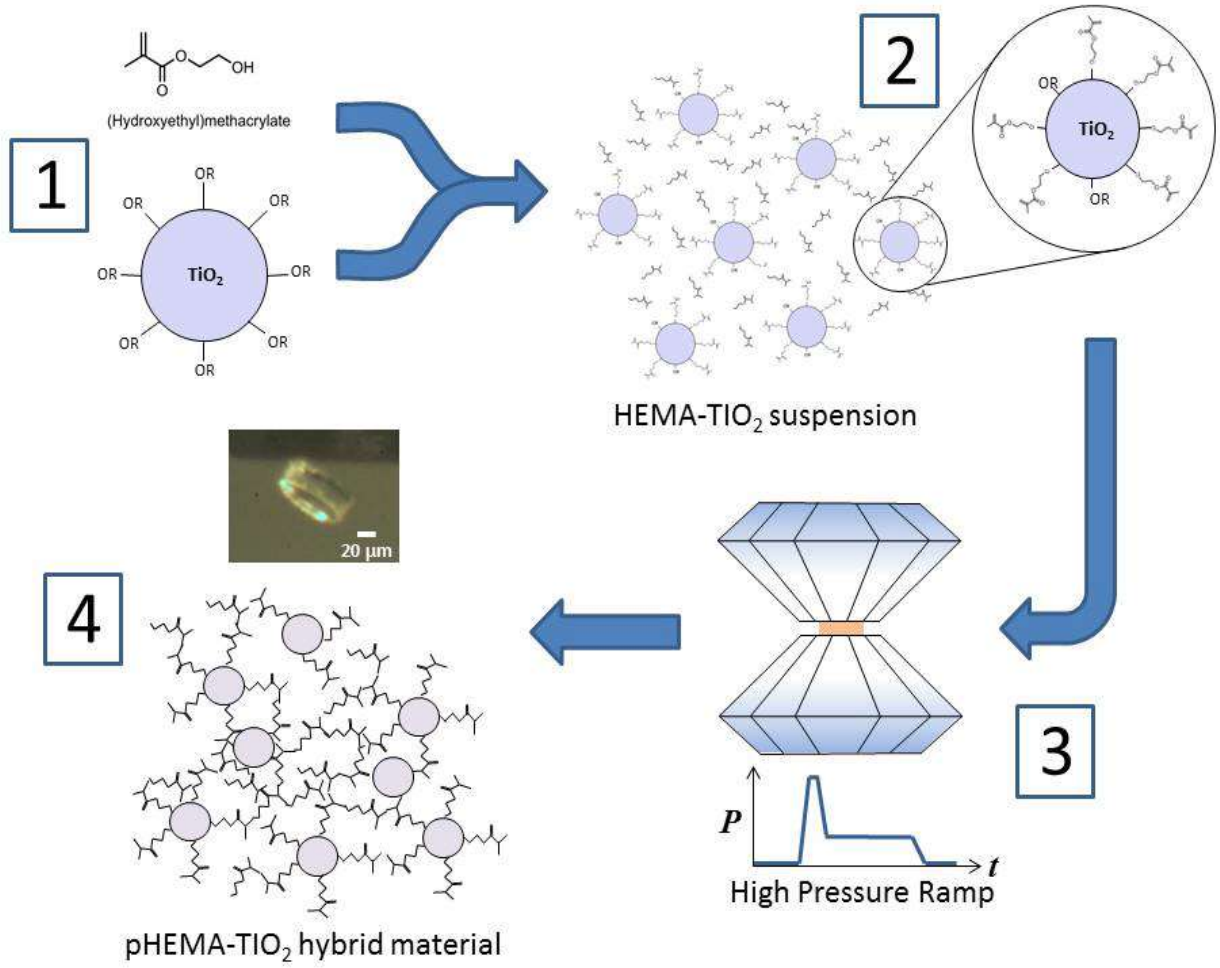

Figure 1: Scheme of the elaboration process of pHEMA-TiO_2 hybrid material by the HPR induced polymerization. (1) synthesis of nanoparticles, (2) surface exchange with the monomers, (3) polymerization induced by high pressure ramp, (4) recovered samples (see text for more details).

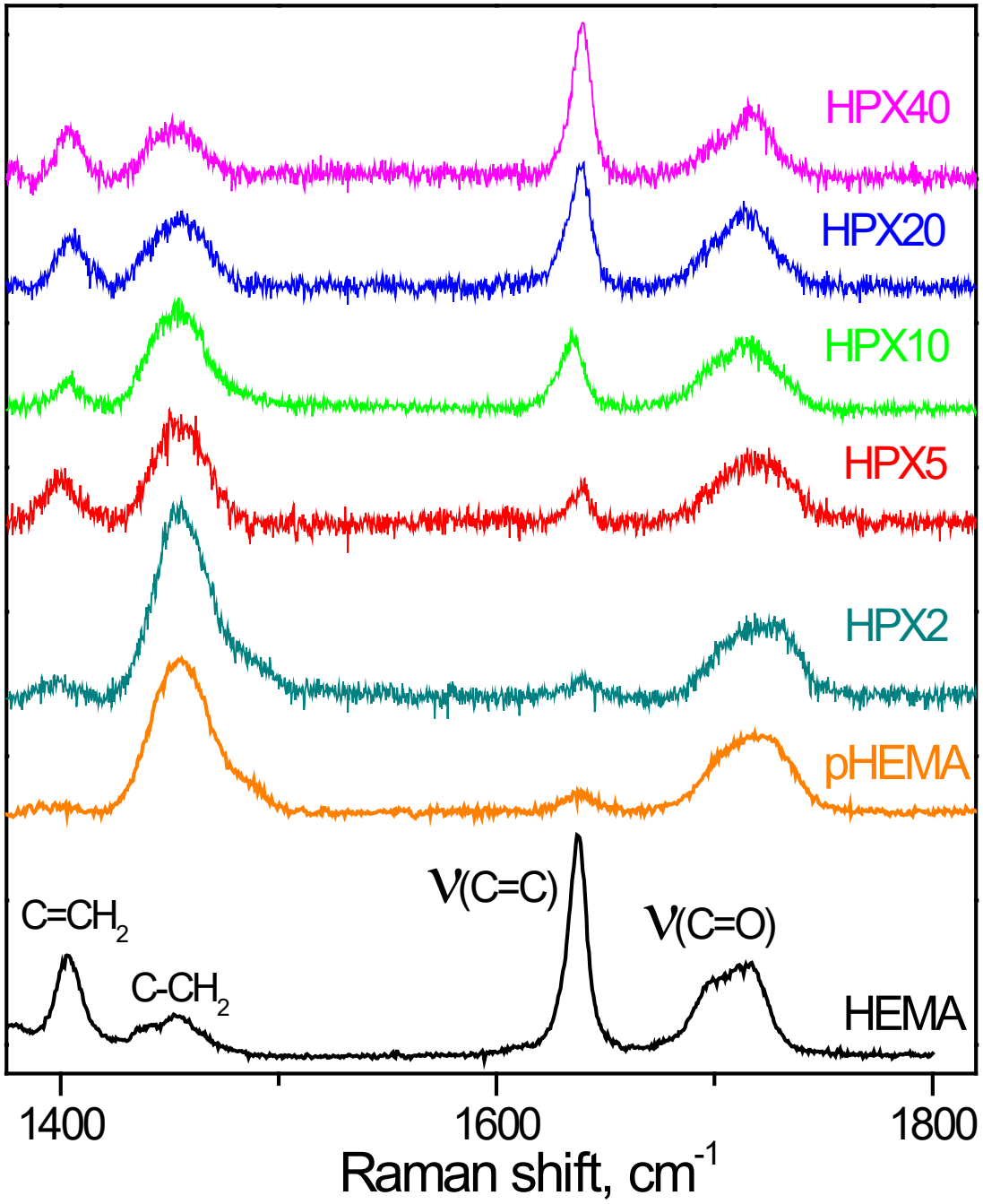

Figure 2 : Raman spectra of liquid HEMA at atmospheric pressure, pHEMA obtained by the HPR process and pHEMA-TiO_2 hybrid materials with different concentrations in TiO_2 nanoparticles prepared by the HPR process. Details regarding the different pHEMA-TiO_2 hybrid samples are given in Table 1

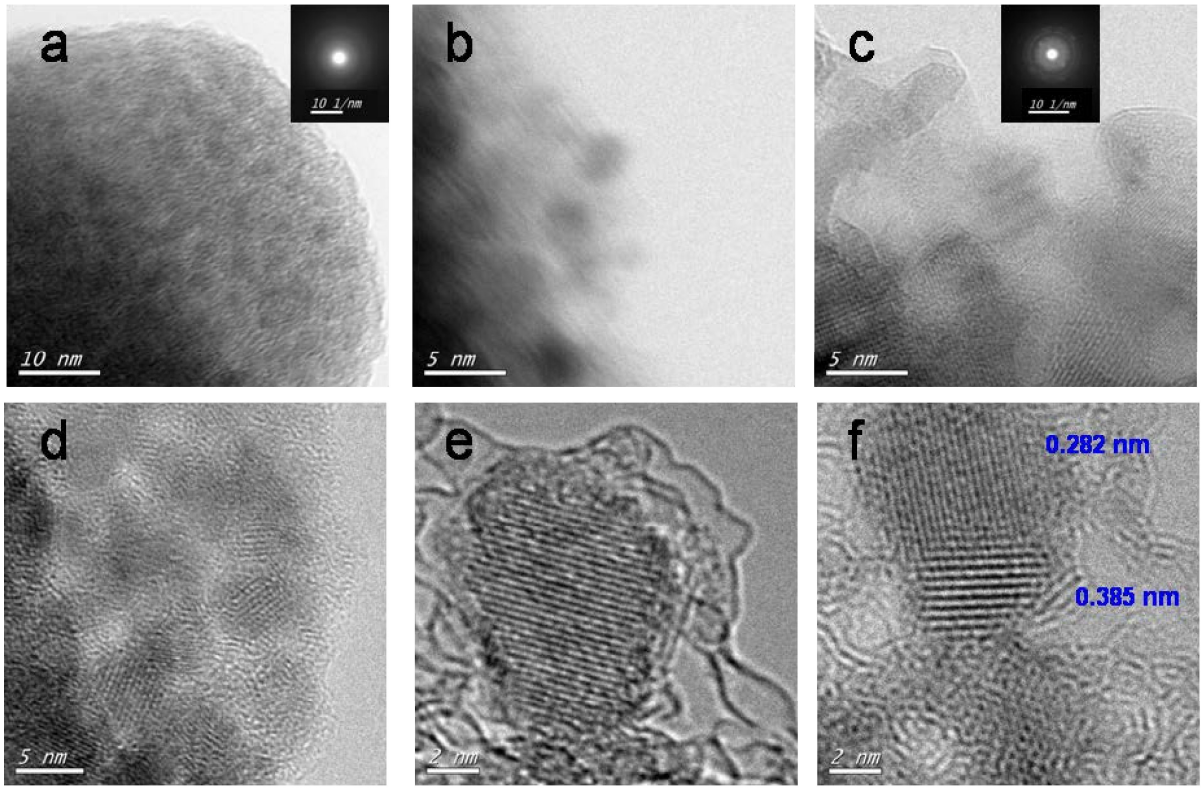

Figure 3: TEM images of pHEMA-TiO_2 hybrid samples synthesized by the HPR induced polymerization: x5 (a), x10 (b, c) and x40 (d-f). Electron diffraction patterns are shown in insets of (a) and (c).

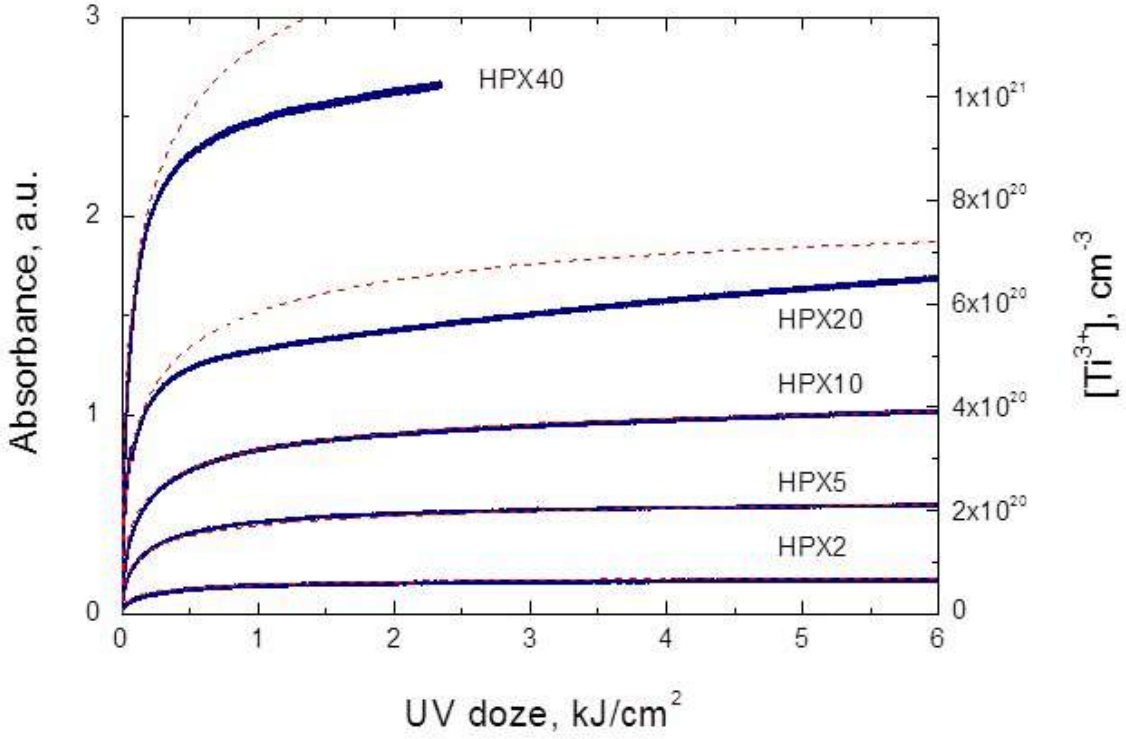

Figure 4: UV laser-induced darkening kinetics (355 nm, 7ns, 4kHz and 10 mJ/cm^2) of nanoparticulate pHEMA-TiO_2 hybrids prepared via the HPR process. The dashed lines are fits of the experimental data using the model described in the text.

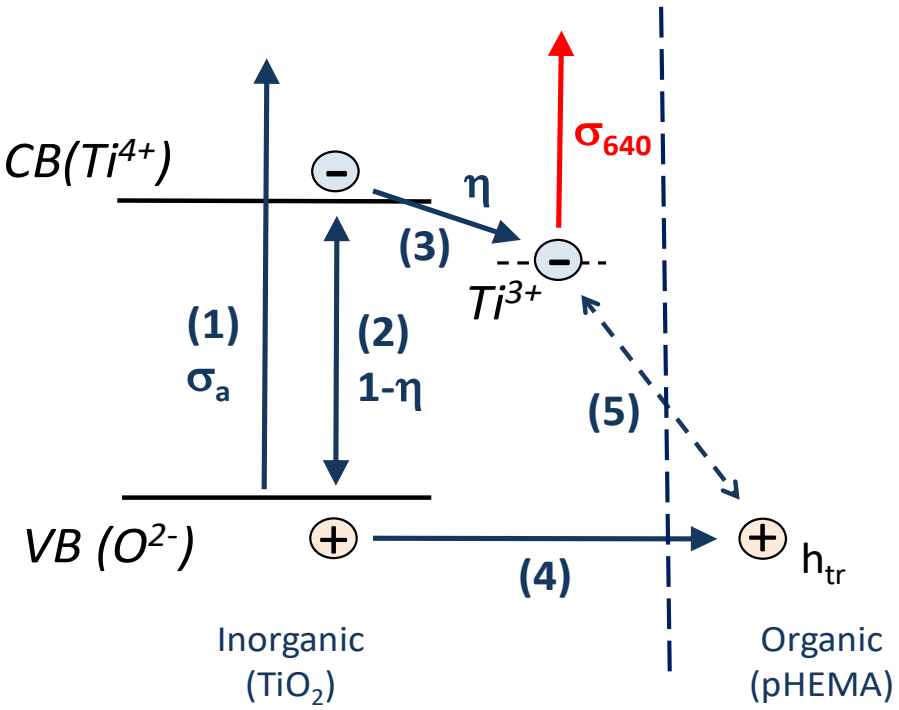

Figure 5: Scheme of the relevant photo-induced processes in the TiO_2 hybrids. The absorption of the probe beam by Ti^{3+} center is represented by a red arrow.

Synthesis of organic-inorganic hybrids via high-pressure-ramp process: Effect of inorganic nanoparticles loading on structural and photochromic properties

E. Evlyukhin [a], L. Museur [a], A. P. Diaz-Gomez-Trevino [b], M. Traore [b], O. Brinza [b], A. Zerr [b], A. Kanaev [b]*

a) Laboratoire de Physique des Lasers - LPL, CNRS UMR 7538, Université Paris 13, Sorbonne Paris Cité, 93430 Villetaneuse, France.

b) Laboratoire des Sciences des Procédés et des Matériaux - LSPM, CNRS, Université Paris 13, Sorbonne Paris Cité, 93430 Villetaneuse, France.

Corresponding Author

* luc.museur@univ-paris13.fr

00 33 1 49 40 37 24

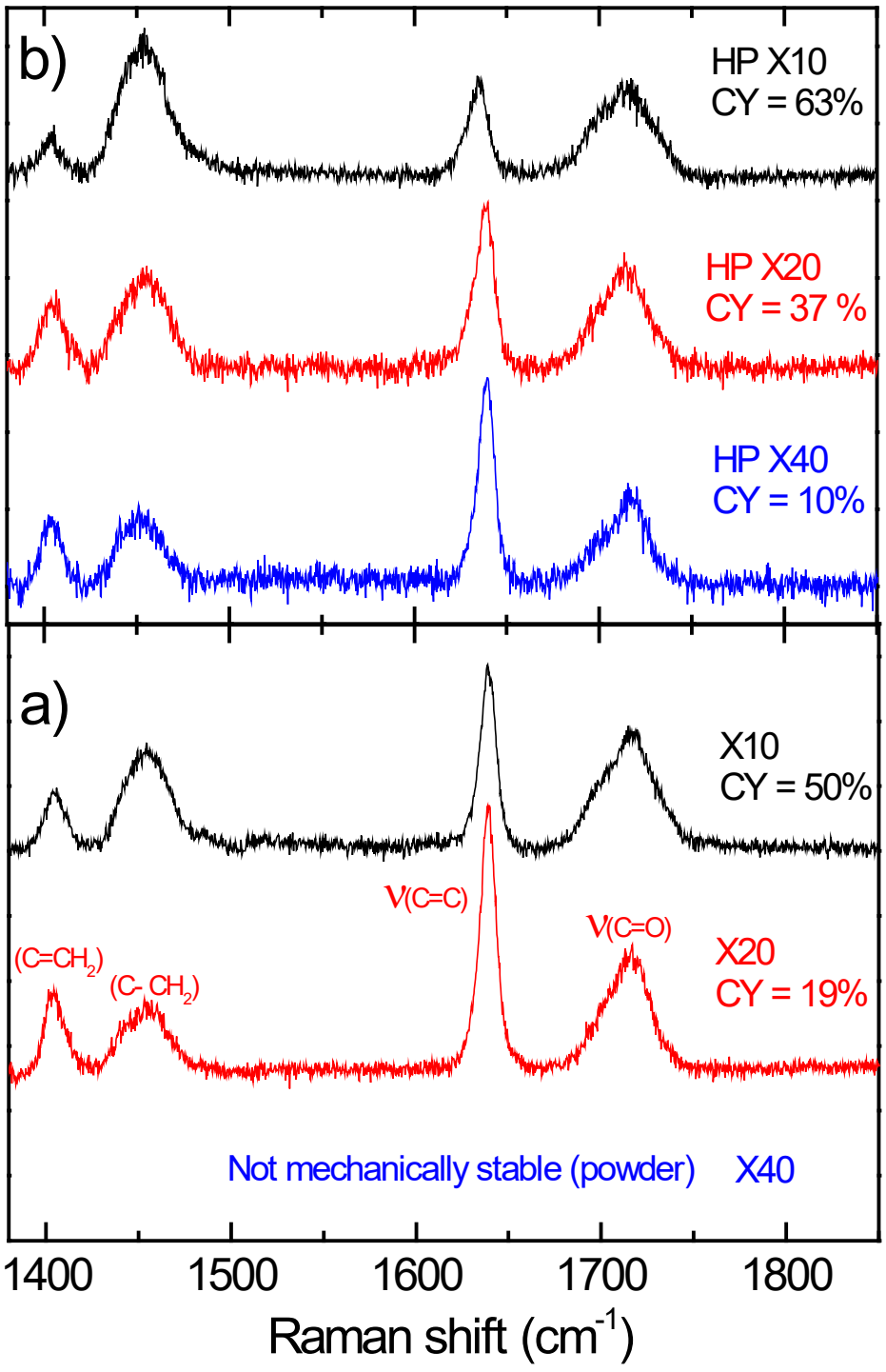

Supplementary Figure 1: Comparison of Raman spectra of pHEMA-TiO_2 hybrids (a) synthetized at ambient pressure with a thermal initiator (AIBN) and (b) synthesized using the HPR induced polymerization.

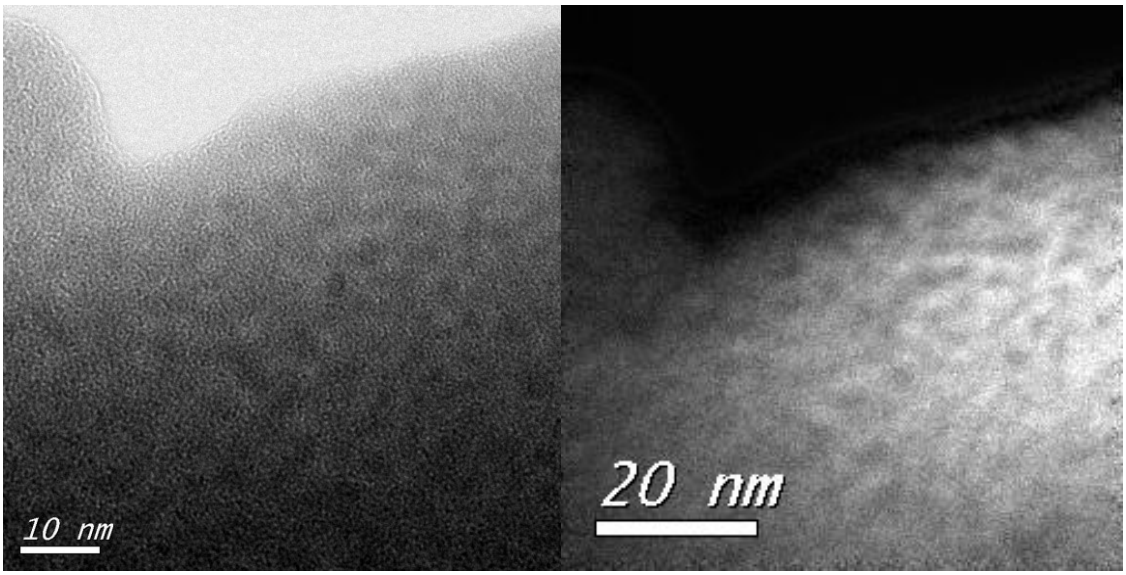

Supplementary Figure 2: HRTEM image of sample HPX5 (right). Energy filtered (Ti) TEM image of the same sample HPX5 (left).

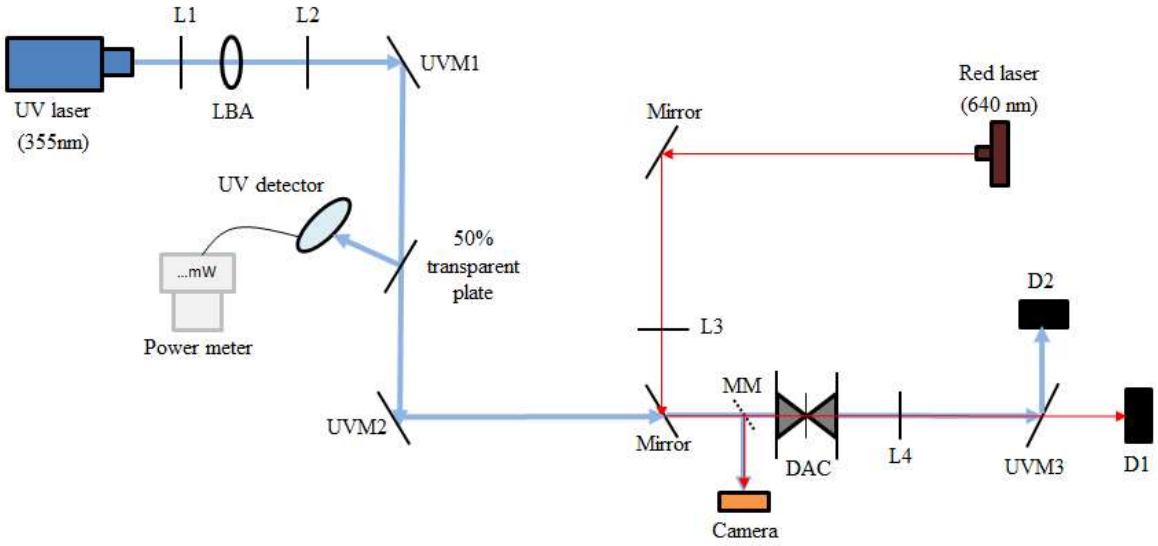

Supplementary Figure 3: Experimental setup of the pump-probe photodarkening experiment.